Temperature and time effect of thermal aging treatment on microstructure and corrosion resistance of UNS S31803 duplex stainless steel

Efeito da temperatura e do tempo de tratamento térmico de envelhecimento na microestrutura e resistência à corrosão do aço inoxidável duplex UNS S31803

Efecto de la temperatura y del tiempo del tratamiento térmico de envejecimiento en la microestructura y la resistencia a la corrosión del acero inoxidable dúplex UNS S31803

Isabela Dainezi
ORCID: https://orcid.org/0000-0002-5937-2859
Federal University of São Carlos, Brazil
Federal University of Alfenas, Brazil
E-mail: beladainezi@gmail.com
Spyridion Haritos Borges
ORCID: https://orcid.org/0000-0002-4071-7546
Federal University of Alfenas, Brazil
E-mail: spyridion.hb@gmail.com
Lucíola Lucena de Sousa
ORCID: https://orcid.org/0000-0001-7494-052X
Federal University of Alfenas, Brazil
E-mail: luciolalucena@gmail.com
Neide Aparecida Mariano
ORCID: https://orcid.org/0000-0001-8345-1808
Federal University of Alfenas, Brazil
E-mail: neide.mariano@unifal-mg.edu.br

Abstract
Duplex stainless steels correspond to a class of steel in which the microstructure is composed basically by the phases ferrite and austenite. Given the metastable character of ferrite, associated phase transformations can occur during thermal treatments, which can lead to a reduction in corrosion resistance. Therefore, the aim of this work was to evaluate the influence of the solution-treated at 1100°C for 30min and aging at 500 and 600°C for 1, 3 and 12h, on the microstructure and corrosion resistance of DSS UNS S31803. The steels were characterized by SEM, EDS, XRD, hardness, microhardness and thermal analysis. The steels aged at 500°C for 1h presented the phase alpha line dispersed in the ferrite, and the steels aged at 600°C for 12h presented the phases alpha line, sigma and chi. In the assays of double cycle potentiodynamic reactivation in solution of 0.5M H_2SO_4 and 0.01M KSNC, it was observed that no sensitization occurred. Furthermore, in the tests of cyclic potentiodynamic polarization, in 3.5% NaCl solution, it was verified that the precipitation of the alpha line phase did not alter corrosion resistance; nevertheless, the sigma phase reduced corrosion resistance.
Keywords: Duplex stainless steel; Corrosion; Phase transformation; Aging.

Resumo
Aços inoxidáveis duplex (AID) correspondem à uma classe de aço em que a microestrutura é composta basicamente pelas fases ferrita e austenita. E devido ao caráter metaestável da ferrita, transformações de fases associadas podem ocorrer durante tratamentos térmicos como alfa linha e sigma, as quais podem levar a diminuição da resistência à corrosão. Dessa forma, o objetivo deste trabalho foi avaliar a influência dos tratamentos térmicos de solubilização a 1100°C por 30min e envelhecimento a 500 e 600°C por 1, 3 e 12h, na microestrutura e na resistência à corrosão do AID UNS S31803. Os aços foram caracterizados por MEV, EDS, DRX, dureza, microdureza e análise térmica, e observou-se que os aços tratados termicamente por envelhecimento apresentaram fração volumétrica de ferrita menor que do aço solubilizado. E os aços envelhecidos a 500°C por 1h apresentaram a fase alfa linha dispersa na ferrita e os aços envelhecidos a 600°C por 12h, apresentaram as fases alfa linha, sigma e chi. Nos ensaios reativação potenciodinâmico duplo ciclo em solução de 0.5M H_2SO_4 e 0.01M KSNC, observou-se que não ocorreu a sensitização. E nos ensaios de polarização potenciodinâmica cíclica, em solução 3.5% NaCl, verificou-se que a precipitação da fase alfa linha não alterou a resistência à corrosão, porém a fase sigma reduziu a resistência à corrosão.
Palavras-chave: Aço inoxidável duplex; Corrosão; Transformação de fases; Envelhecimento.

Resumen

Los aceros inoxidables dúplex (AID) corresponden a una clase de acero en la que la microestructura está compuesta básicamente por las fases ferrita y austenita. Y debido al carácter metaestable de la ferrita, pueden ocurrir transformaciones en las fases asociadas durante los tratamientos térmicos como la línea alfa y sigma, lo que puede conducir a una disminución de la resistencia a la corrosión. Así, el objetivo de este trabajo fue evaluar la influencia de los tratamientos térmicos de solubilización a 1100°C durante 30min y envejecimiento a 500 y 600°C durante 1, 3 y 12h, sobre la microestructura y resistencia a la corrosión de AID UNS S31803. Los aceros se caracterizaron por SEM, EDS, DRX, dureza, micro dureza y análisis térmico, y se observó que los aceros tratados térmicamente por envejecimiento presentaban una fracción volumétrica de ferrita menor que el acero solubilizado. Y los aceros envejecidos a 500 ° C durante 1h presentaron la fase de línea alfa dispersa en ferrita y los aceros envejecidos a 600 ° C durante 12h presentaron las fases de línea alfa, sigma y chi. En los ensayos de reactivación potencio dinámica de doble ciclo en una solución de H_2SO_4 0,5 M y KSNC 0,01M, se observó que no se produjo sensibilización. Y en las pruebas de polarización potencio dinámica cíclica, en una solución de NaCl al 3,5%, se encontró que la precipitación de la fase de línea alfa no cambiaba la resistencia a la corrosión, pero la fase sigma reducía la resistencia a la corrosión.

Palabras clave: Acero inoxidable dúplex; Corrosión; Transformación de fase; Envejecimiento.

1. Introduction

Duplex stainless steels (DSS) present low carbon content because of the process of decarburization by oxygen blowing associated to the argon used in its production, which, associated to a biphasic microstructure, composed of ferrite (α) and austenite (γ), promote high corrosion resistance, good weldability, besides high mechanical resistance. Nevertheless, the typical microstructure can be modified by the thermal treatments of solubilization and aging (Örnek, Burke, Hashimoto, Lim & Engelberg, 2017, Sicupira, Cardoso Junior, Bracarense, Frankel & Lins, 2016).

The thermal treatment of solubilization aims at adjusting the volumetric fractions between the phases α and γ, by the growth of the austenite grains, and at solubilizing intermetallic phases present in steel, such as sigma (σ), chi (χ) and alpha line (α') (Örnek & Engelberg, 2015, Sáenz *et al.*, 2020, Zeng, Yang, Xu, Xin & Li, 2019, Zhang *et al.*, 2017). The thermal treatment of solubilization is usually performed between 1000-1200°C, followed by cooling in water, to avoid the precipitation of undesirable intermetallic phases (Arturo, Hugo, Rafael, Egberto & Antonio, 2015, Majid & Shahi, 2020, Sáenz *et al.*, 2020, Zeng *et al.*, 2019). The thermal treatment of aging aims at promoting the precipitation of intermetallic phases such as α', σ and χ, and it can be performed after the thermal treatment of solubilization, for the steel to present only the desired phases according to the application (Berecz, Fazakas, Mészáros & Sajó, 2015, Chail & Kangas, 2016, Cronemberger *et al.*, 2014, Cronemberger, M. E. R., Nakamatsu, S., Rovere, C. A. D., Kuri, S. E. & Mariano, N. A., 2015).

Phase α' is a precipitate rich in chromium and it occurs inside α, it presents a body-centered cubic (BCC) structure, coherent with the ferritic matrix, and since it has low energy of interface with the ferritic matrix, it presents high resistance to coalescence (Chen & Limin, 2015, Cronemberger *et al.*, 2015, Hilders, Zambrano & Ochoa, 2018, Jinlong, Tongxiang, Lacerda, Cândido, & Godefroid, 2015). The precipitation of phase α' is associated to the diffusion of chromium and, therefore, it promotes the formation of regions poor in chromium around it. Thus, DSS becomes more susceptible to the localized corrosion, for being sensitive to active dissolution and contributing to the degradation of passive film stability (Hilders *et al.*, 2018, Jinlong *et al.*, 2015, Lacerda *et al.*, 2015, Li, Lo, Kwok, Sun & Lai, 2018, Mandal, 2016, Mohammed, Shrikrishna & Sathiya, 2016, Verma & Taiwade, 2017).

Furthermore, the formation of α' causes a cross-stich displacement, leading to a decreased mobility of disagreements, leading to an increase in hardiness, in the yield point and mechanical resistance, besides reducing toughness and elongation (Appleton, 2019, Llorca-Isern, López-Jiménez, López-Luque, Biezma & Roca, 2016, Mandal, 2016, Marques, Silva & Santos, 2020, Mohammed *et al.*, 2016, Paulraj & Garg, 2015, Rezende *et al.* 2018, Rezende, Dainezi, Apolinario, Sousa & Mariano, 2019, Silva *et al.*, 2016, Rivolta, Gerosa & Tavasci, 2018, Silva *et al.*, 2016, Verma & Taiwade, 2017).

Phase α' can be formed by two mechanisms, nucleation and growth, and spinodal decomposition of ferrite, depending

on the chemical composition of the ferrite phase and the temperature of the treatment. Both mechanisms occur to reduce the Gibbs free energy of the system and, consequently, promote a thermodynamically more stable state (Appleton, 2019, Llorca-Isern *et al.*, 2016, Marques *et al.*, 2020, Mohammed *et al.*, 2016, Paulraj & Garg, 2015, Rezende *et al.* 2018, Rivolta *et al.*, 2018, Silva *et al.*, 2016, Verma & Taiwade, 2017).

The mechanism of nucleation and growth occurs when the chromium content in the ferrite phase is inferior to 23% (mass) and the thermal treatment of aging is performed above 500°C. For this mechanism, the diffusion occurs with a greater reduction in the Gibbs free energy and phase α' is more roughly formed than in the spinodal decomposition, because of the formation of coherent interfaces (Cavalcanti, Muterlle & Reinke, 2019, Haupt, Silva, Falcade, Santos & Reguly, 2019, Kisasoz, Gurel & Karaaslan, 2016, Mehta, Jadhav, Shaikh, Kumar & Kirwai, 2019, Nithin, Sekar & Joseph, 2019, Ogawa & Osuki, 2020, Powar, Gujar, Manthani, Pawar & Singh, 2017, Valeriano, Correa, Mariano, Robin & Machado, 2019).

The mechanism of spinodal decomposition of ferrite occurs when the chromium content is superior to 23% (in mass) and the thermal treatment of aging is performed at 280-475°C (Hilders *et al.*, 2018, Jinlong *et al.*, 2015, Lacerda *et al.*, 2015, Li *et al.*, 2018). The condition for spinodal decomposition to occur is that the alloy composition be the one in which the curve of free energy presents a negative curvature, in other words: $\partial^2 G / \partial \chi^2 < 0.$

This condition is observed for systems at low temperatures and where mixing enthalpy is positive, in other words, ΔHmix > 0. This last factor occurs because of a characteristic of atoms of having more favorable ligations among equal species than different species. Thus, when chemical composition and temperature are located inside the chemical spinodal, phase α is unstable, there is no nucleation barrier, and decomposition occurs in diffusion of the "up-hill" type, nucleating phase α', by spinodal decomposition.

Nonetheless, in case the composition is inside the miscibility GAP and outside the chemical spinodal, phase α is metastable; thus, there might occur the formation of phase α', by nucleation and growth, and the diffusion is of the "down-hill" type.

Phase sigma derives from a reaction in the eutectoid, in which the ferrite phase is decomposed into sigma and secondary austenite ($\alpha \to \sigma + \gamma_2$) (Majid & Shahi, 2020, Örnek & Engelberg, 2015, Sáenz *et al.*, 2020, Zeng *et al.*, 2019). This reaction is started around the grains α/γ or α/α, and the consumption of the ferrite phase grows. Its precipitation occurs by the diffusion of the elements chromium, molybdenum and silicon, and with this, there is the formation of regions poor in these elements, leaving DSS with lower corrosion resistance, besides reducing ductility and toughness (Deng & Zheng, 2019, Dille *et al.*, 2017, Matias, Tavares, Pardal & Ribeiro, 2017, Mehta *et al.*, 2019, Nithin *et al.*, 2019, Ogawa & Osuki, 2020, Xiang, Liu, Silva *et al.*, 2016).

Phase chi is thermodynamically unstable and is usually precipitated around the grains α/γ or α/α (Örnek *et al.*, 2017). Usually, phase chi is consumed by the phases sigma and austenite, and this tends to weaken and reduce the localized corrosion resistance of DSS (Alvarez-Armas & Degallaix-Moreuil, 2009, Martins & Hara, 2004, Morais & Magnabosco, 2017, Silva *et al.*, 2016, Santos & Magnabosco, 2015, Warren *et al.*, 2015).

Therefore, the aim of this work was to evaluate the influence of the thermal treatments of solubilization and aging on phase precipitation and electrochemical corrosion behavior, employing the techniques of cyclic potentiodynamic polarization and by the double cycle potentiodynamic reactivation (DL-EPR).

2. Methodology

The research methodology applied in this study is experimental/laboratory, relying on quantitative and qualitative approaches, as it is aimed at testing hypotheses in numerical and observed forms about the phase transformation resulting from

the aging heat treatment (Ludke & Andre, 2013, Koche, 2011, Pereira, Shitsuka, Parreira & Shitsuka, 2018). Thus, the set of analyzes used to measure the influence of the phase transformation phenomenon occurring in duplex stainless steel about the modification of its corrosion resistance is described below.

The nominal chemical composition of the steel studied was determined by inductively coupled plasma atomic emission spectroscopy and is presented in Table 1.

Table 1: Nominal chemical composition of duplex stainless steel (wt.%).

Cr	Ni	Mo	Mn	Si	N	C	Fe
23.0	5.5	3.15	1.97	0.45	0.17	0.015	bal.

Source: Authors (2021).

The samples were solution-treated at 1100ºC for 30 min and cooled in water. After that, aging treatments were performed at 500 and 600ºC for 1, 3 and 12h, followed by cooling in water.

The samples were analyzed by scanning electron microscopy (SEM) and the semi-quantitative microanalysis of the phases was obtained by energy-dispersive spectroscopy (EDS), after chemical attack with Behara (2.02M HCl and 0.045M $K_2S_2O_5$).

X-ray diffraction (XRD) analysis was performed with Cu Kα radiation, in a range of 2θ from 40º to 100º, with a step of 0.02º for 2 s/step.

Thermal analysis was performed using differential scanning calorimetry (DSC) in the equipment Netzsch Júpiter STA 449F3, the samples were submitted to heating from 30ºC to 1200ºC, at a heating rate of 5ºC/min, under an argon and nitrogen atmosphere.

The corrosion behavior was evaluated by the cyclic potentiodynamic polarization method using a potentiostat Metrohm model Autolab/PGSTART 302 connected to a typical electrochemical cell with a saturated calomel electrode (SCE) used as a reference electrode, a platinum plate employed as counter-electrode and the working electrode made from the steel studied. Electrochemical measurements were performed in triplicate for each condition. The electrolyte used was 3.5 % sodium chloride solution at 25ºC. The potentiodynamic curves were measured at a potential scan rate of 1mV/s in the range from -1.5V, with reversion of the direction when the anodic current density of 10^{-3} A/cm^2 was reached.

The corrosion tests by double cycle potentiodynamic reactivation (DL-EPR) were performed in the solutions 0.5M H_2SO_4 and 0.01M KSNC. The DL-EPR curves were obtained by scanning the potential from 0.5 to 0.3V, the scan was reversed and swept from positive to negative potentials at -0.5V at a constant rate of 2mV/s.

The corrosion tests were performed in the samples in which there was precipitation of the alpha line phase, to evaluate its effect in relation to the samples under the conditions as-received and solubilized.

The microhardness (HV) test was performed with a load of 0.1 kgf and printing time of 15 seconds, and hardness (HRC) was also determined with a conical penetrator of 120° and load of 150kgf. Ferritoscopy assay was also performed for the DSS samples under the conditions studied.

3. Results and Discussion

The micrograph of the DSS UNS S31803 as received are shown in Figure 1a, and in the regions indicated by A and B, the EDS analyses were performed. The austenite phase was observed in the form of elongated islands, and in alternate regions of refined and acicular structures, dispersed in the ferritic matrix. Figure 1b shows a micrograph of UNS S31803 solution-

treated at the temperature of 1100°C for 30 min and cooled with water.

Figure 1: Micrographs obtained by SEM of duplex stainless steel DSS UNS S31803. (a) As-received; (b) Solution-treated at1100°C for 30 min and cooled in water.

(a)   (b)
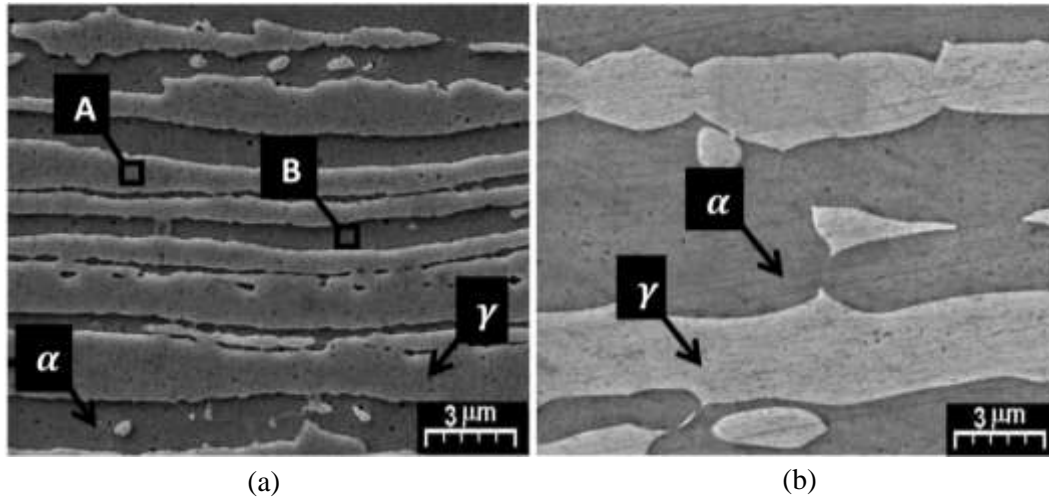
Source: Authors (2021).

The austenite is observed in the form of lamella islands, distributed in the ferritic matrix. It is noted that the solution-treated resulted in a microstructure with homogeneous distribution between the phases and there was the growth of austenite, because of the diffusion of gammagenic alloy elements such as Ni, C and Mn.

The duplex microstructure is formed during cooling, and firstly, austenite presents the Widmanstätten morphology inside and around the grains of ferrite; subsequently, it undergoes transformation in state by the diffusion of alloy elements and displacement of interfaces, imposing an orientation relationship of the type Kurdjumov-Sachs (K-S) or Nishiyama-Wasserman (N-W) between the new austenite and the precursor ferrite, generating semi-coherent interfaces (Alvarez-Armas & Degallaix-Moreuil, 2009).

Austenite stringers around the ferrite grains maintain this type of orientation relationship with one of the ferrite grains, whereas the other interface has an incoherent limit. The result is a distribution of austenite monocrystals in the form of plates oriented in space almost at random within a ferrite matrix (Alvarez-Armas & Degallaix-Moreuil, 2009).

Figures 2a, 2b and 2c show DSS UNS S31803 micrographs, under the condition aged at 500°C for 1, 3 and 12h, respectively. It is observed that the thermal treatment of aging performed at 500°C for 1h (Figure 2a) was able to precipitate phase α', inside the ferrite, by the mechanism of nucleation and growth. The morphology of phase α' is a consequence of the differences between the thermal expansion of ferrite and of α', besides the proximity between the network parameters between the matrix and the precipitate which led to the formation of coherent interfaces and a spherical appearance with diameters of approximately 100nm. Furthermore, it is noted by Figures 2b and 2c that there was a growth of the austenite grains because of the diffusion of the alloy elements, analogously to the observed after the solution-treated, Figure 1b.

Figure 2: Micrographs of DSS UNS S31803, under the conditions aged at 500°C. (a) Aging time of 1h; (b) Aging time of 3h; (c) Aging time of 12h.

(a)

(b)

(c)
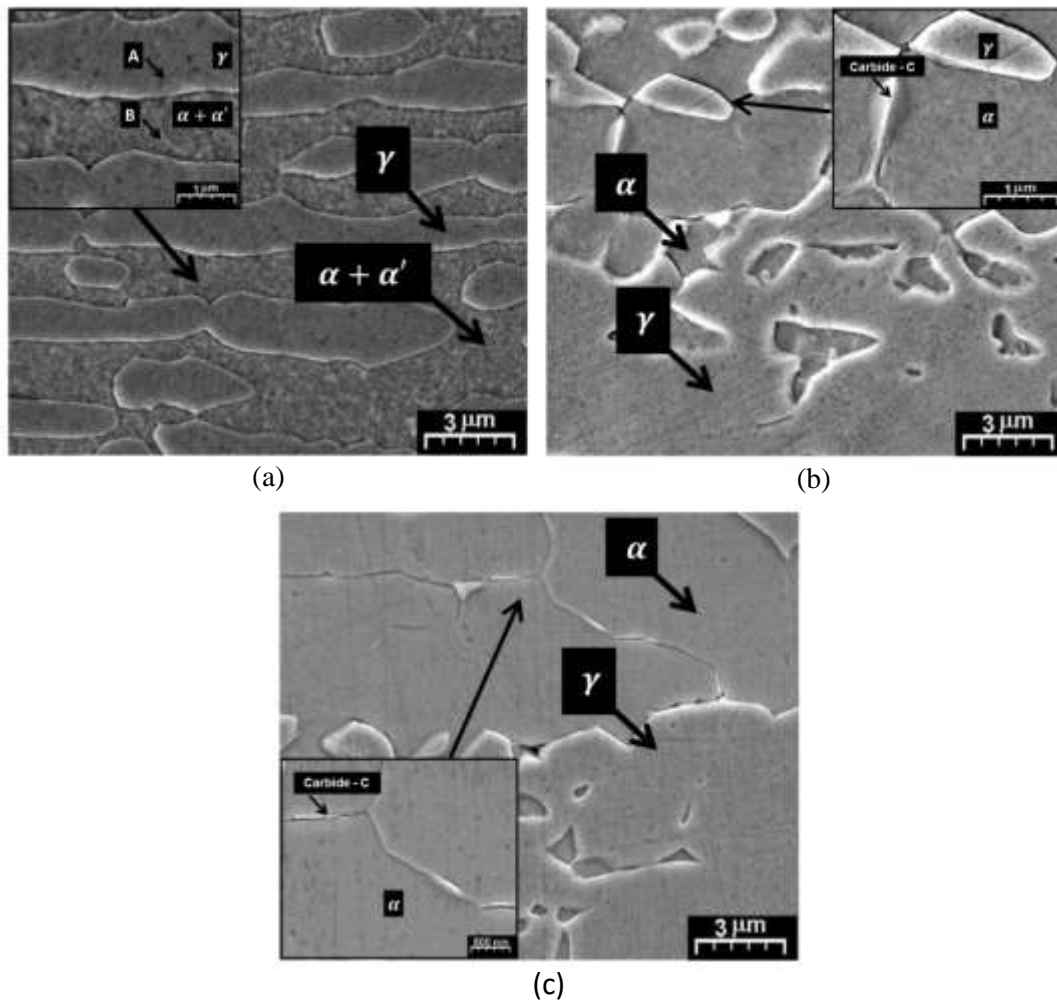
Source: Authors (2021).

The micrographs obtained by scanning electron microscopy for UNS S31803 aged at 600°C for 1, 3 and 12h are shown in Figure 3. An alteration in austenite morphology was observed in the three times of aging treatment, changing from elongated islands to a massive structure, deriving from the growth of the austenite grains followed by their union, promoting a heterogeneous microstructure. The treatment of aging at 600°C for 12h promoted the precipitation of phase α', by the method of nucleation and growth, with morphology similar to the treatment of aging at 500°C for 1h (Figure 2a).

Figure 3: Micrographs of DSS UNS S31803, under the condition aged at 600°C. (a) Aging time of 1h; (b) Aging time of 3h; (c) Aging time of 12h.

(a)

(b)

(c)
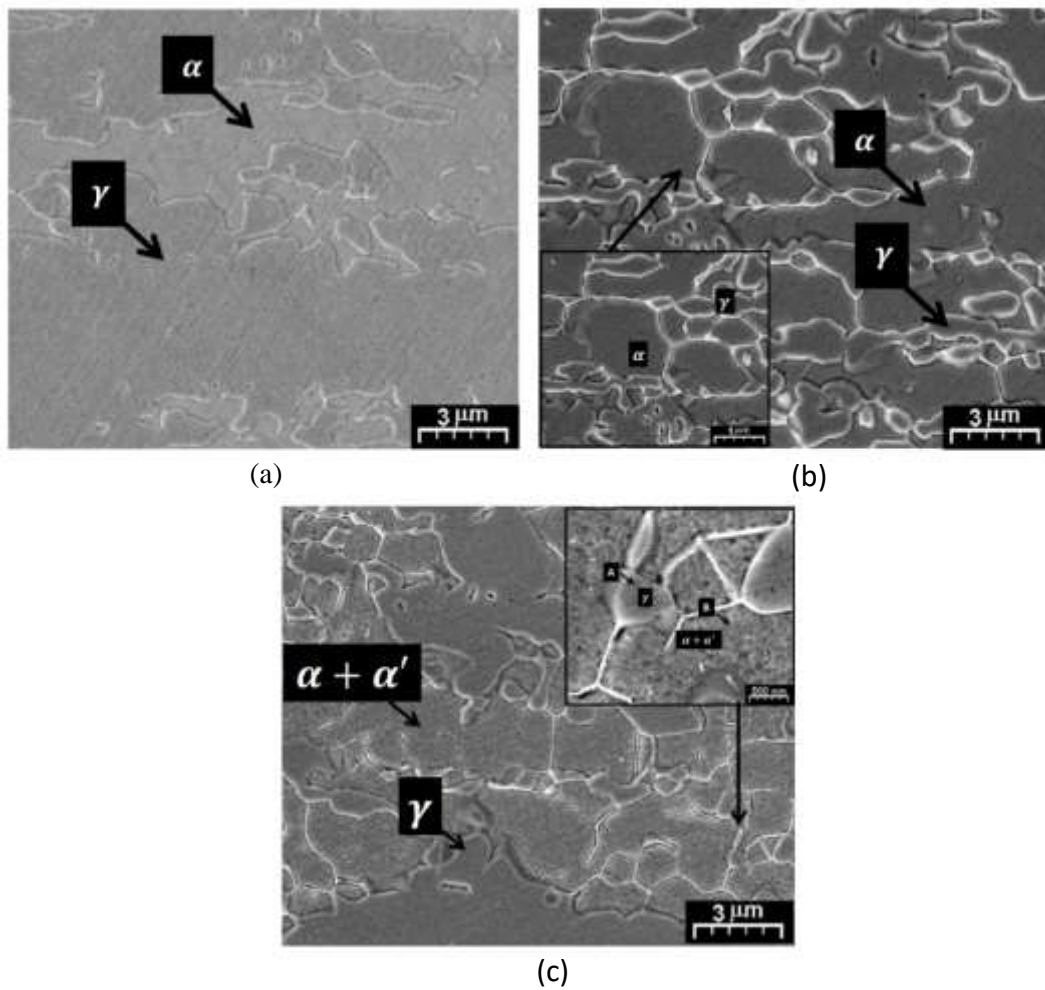
Source: Authors (2021).

The results of the semiquantitative microanalyses by energy-dispersive spectroscopy (EDS) in the regions A (phase γ) and B (phase α), under the conditions as-received, solution-treated, aged at 500°C for 1 and 600°C for 12h are shown in Table 2.

Table 2: Semiquantitative microanalysis by EDS under the conditions as-received, solution-treated and aging at 500°C for 1h and 600°C for 12h (in % mass).

DSS UNS S31803	Phases	Fe	Cr	Ni	Mo
As-received	α	62.95	24.43	5.01	5.23
	γ	65.74	22.28	7.07	2.98
Solution-treated at 1100ºC	α	64.87	24.23	4.41	4.30
	γ	66.13	21.49	6.86	2.50
Aged at 500°C for 1h	α + α'	61.04	23.89	4.82	6.71
	γ	63.43	20.57	7.31	4.06
Aged at 600°C for 12h	α + α'	61.69	24.15	4.78	6.55
	γ	65.31	22.12	7.39	4.26

Source: Authors (2021).

It is observed that the alloy elements chromium and molybdenum are majoritarian in the ferrite phase, because of the ferritizing character of these elements, whereas the alloy element nickel is majoritarian in austenite, given the austenitizing character. It was also observed that there were no significant variations in the contents of chromium, molybdenum and nickel under the studied conditions, even with the precipitation of phase α' inside ferrite.

Figure 4 presents the X-ray diffraction spectra of DSS UNS S31803 under the studied conditions. It was observed that the solution-treated the intermetallic phases σ and χ present under the condition as-received. Furthermore, the precipitation of phase σ was observed, in the thermal treatments of aging performed at 500°C for 1h and at 600°C at the times of 1, 3 and 12 h, and the precipitation of phase χ, aging at 600°C for 1 hour.

Figure 4: X-ray diffraction spectra of the duplex stainless steels under the conditions. (a) Aged at 500°C; (b) Aged at 600°C.

(a)   (b)
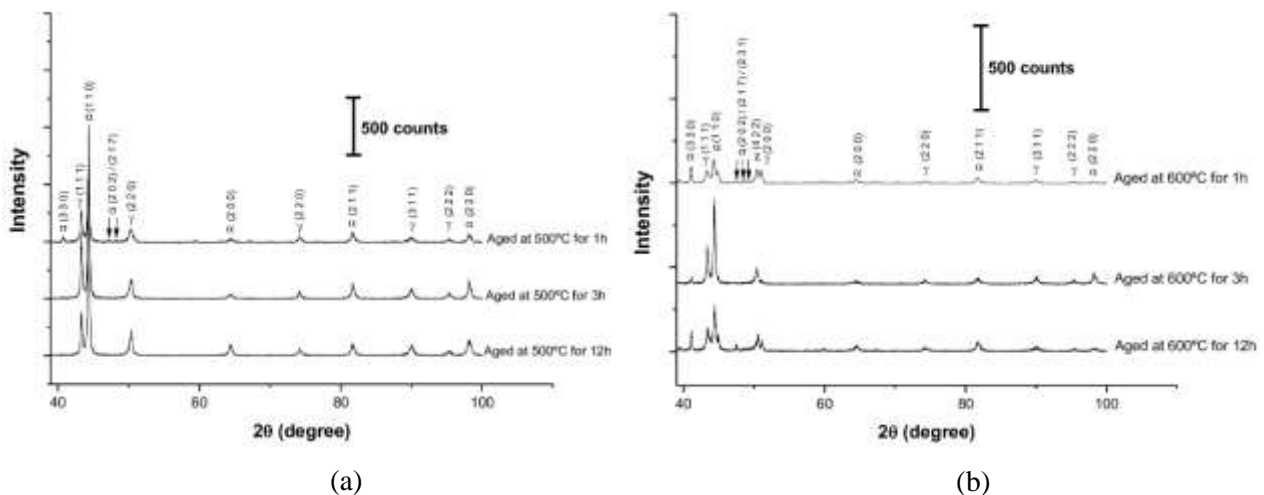
Source: Authors (2021).

Table 3 shows the volumetric fractions of the ferrite phase, measured using a ferritoscope. A decrease in the volumetric fraction of ferrite was observed in the thermal treatments of aging, in relation to the conditions as-received and solubilized, deriving from both the growth of the austenite grains and the precipitation of phases σ and χ, as shown in Figure 4. Phase sigma derives from a reaction in eutectoid, formed by the decomposition of ferrite, leading to the reduction in the

volumetric fraction of ferrite (Alvarez-Armas & Degallaix-Moreuil, 2009).

Table 3: Volumetric fraction of the ferrite phase in DSS UNS S31803.

DSS UNS S31803	Volumetric fraction of the ferrite phase (%)
As-received	41.97 ± 0.96
Solution-treated at1100ºC	41.39 ± 0.72
Aged at 500ºC for 1h	37.85 ± 0.58
Aged at 500ºC for 3h	37.18 ± 0.72
Aged at 500ºC for 12h	30.77 ± 0.98
Aged at 600ºC for 1h	39.88 ± 0.55
Aged at 600ºC for 3h	34.62 ± 0.52
Aged at 600ºC for 12h	36.04 ± 0.72

Source: Authors (2021).

Table 4 shows the hardness values obtained for DSS under the studied conditions, and a decrease in hardness was observed after the solution-treat, deriving from the dissolution of the intermetallic phases σ and γ, present in the as-received steel. In the steel aged at 500°C for 1h, there was the precipitation of phases α' and σ, which present weakening and hardening characteristics, promoting higher hardness, in relation to the aging times of 3 and 12h. The treatment of aging at 500ºC for 1h (Figure 2a) and 600°C for 12h (Figure 3c) promoted the precipitation of phase α', which presents hardening characteristics, which led to an increase in hardness in relation to the other times.

Table 4: Results of DSS UNS S31803 hardness (HRC).

DSS UNS S31803	Hardness (HRC)
As-received	24 ± 1
Solution-treated at 1100ºC	15 ± 2
Aged at 500ºC for 1h	23 ± 1
Aged at 500ºC for 3h	21 ± 1
Aged at 500ºC for 12h	22 ± 1
Aged at 600ºC for 1h	22 ± 1
Aged at 600ºC for 3h	22 ± 1
Aged at 600ºC for 12h	23 ± 1

Source: Authors (2021).

Table 5 shows the microhardness values for the phases ferrite and austenite under the studied conditions. It was observed that after the solution-treated, there was no significant variation in the microhardness values. The ferrite phase presented the highest microhardness values under the conditions of aging at 500°C for 1h (276.8 ± 4.2 HV10) and 600°C for 12h (278.9 ± 2.7 HV10), because of the precipitation of phase α' inside ferrite. It was observed that there was no significant variation in the microhardness values of the austenite phase, suggesting that the precipitation of phase G did not occur inside austenite.

Table 5: Results of the microhardness (HV10) of the phases present in DSS UNS S31803.

DSS UNS S31803	Phase	Microhardness (HV10)
As-received	α	248.6 ± 6.9
	γ	268.6 ± 4.3
Solution-treated at 1100ºC	α	254.4 ± 3.9
	γ	270.8 ± 4.8
Aged at 500°C for 1h	α	276.8 ± 4.2
	γ	271.1 ± 3.1
Aged at 500°C for 3h	α	255.9 ± 3.5
	γ	272.1 ± 3.7
Aged at 500°C for 12h	α	264.7 ± 3.9
	γ	272.6 ± 2.7
Aged at 600°C for 1h	α	253.1 ± 2.4
	γ	271.8 ± 1.7
Aged at 600°C for 3h	α	255.1 ± 3.5
	γ	271.9 ± 1.6
Aged at 600°C for 12h	α	278.9 ± 2.7
	γ	272.2 ± 2.1

Source: Authors (2021).

Figure 5 presents the thermograms of steel DSS UNS S31803, obtained by differential scanning calorimetry (DSC), using nitrogen and argon atmospheres. The presence of an endothermic peak at 428.9°C and 520.4°C was observed in the argon and nitrogen atmospheres, respectively, suggesting the transformation of ferrite into α', because of the decrease in chromium in the ferritic matrix, promoting an increase in ferromagnetic/paramagnetic transition temperature of ferrite. The exothermic peaks at 842.2°C and 860.6°C, in the argon and nitrogen atmospheres, respectively, derives from the consumption of ferrite by paramagnetic phases, such as austenite and σ.

Figure 5: DSC thermogram for DSS UNS S31803 in argon and nitrogen atmospheres.
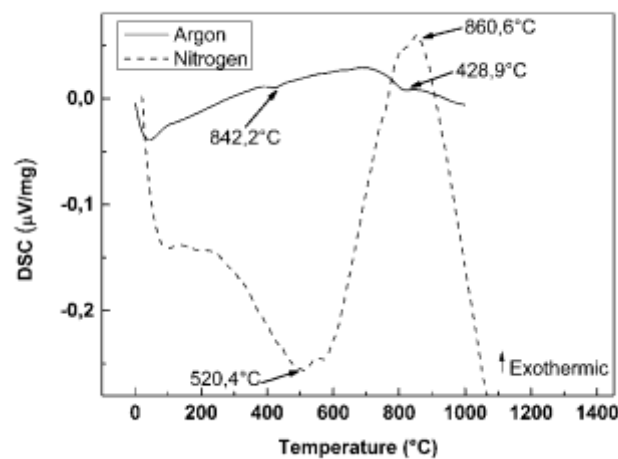
Source: Authors (2021).

Assays of double cycle potentiodynamic reactivation (DL-EPR) and cyclic potentiodynamic polarization (CPP) were performed in a solution of 0.5M H2SO4 and 0.01M KSN, in the samples in which there was precipitation of phase α' (aged at 500°C for 1h and 600°C for 12h) and under the conditions as-received and solubilized, as shown in Figure 6.

Figure 6: Corrosion assay of DSS UNS S31803 in a solution of 0.5M H2SO4 and 0.01M KSNC. (a) Open circuit potential; (b) Double cycle potentiodynamic reactivation.

(a)   (b)
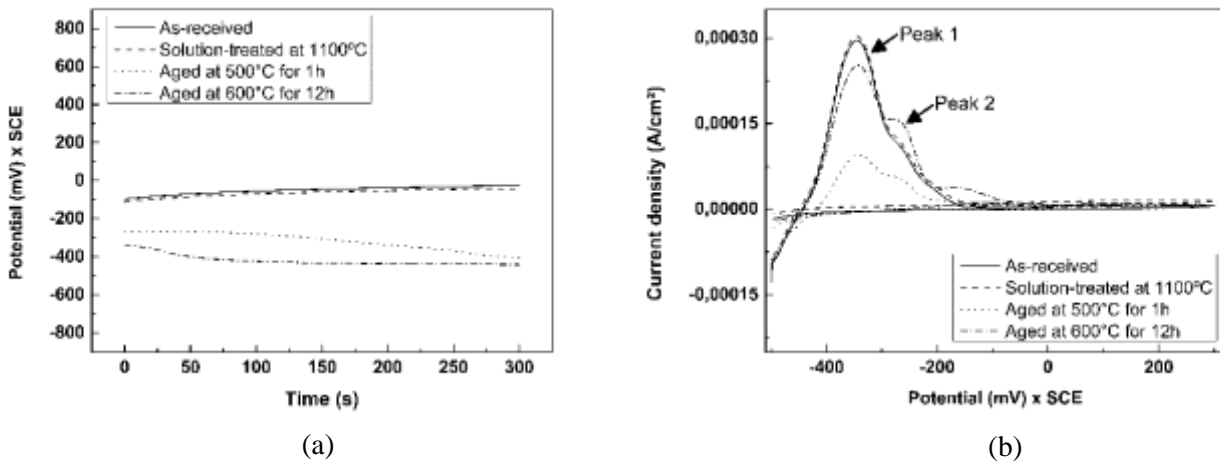
Source: Authors (2021).

The values of corrosion potentials (Ecorr) and degree of sensitization are presented in Table 6. It was observed that under the conditions as-received and solubilized, the values of the potentials increased with time, deriving from the formation of a stable passive layer that adheres to the steel surface. Nevertheless, under the conditions of aging at 500°C for 1h and 600°C for 12h, the values of the potentials decreased over time, followed by a stabilization at the times of 250 seconds and 50 seconds, respectively, evidencing a generalized corrosion followed by the formation of a passive layer.

Table 6: Open circuit corrosion potential and degree of sensitization by double cycle potentiodynamic reactivation, of DSS UNS S31803 in solution of 0.5M H2SO4 and 0.01M KSNC.

DSS UNS S31803	Ecorr (mV)	Degree of sensitization
As-received	-40 ± 2	0.0142 ± 0.0008
Solution-treated at 1100ºC	-44 ± 4	0.0164 ± 0.0004
Aged at 500°C for 1h	-402 ± 7	0.0025 ± 0.0001
Aged at 600°C for 12h	-440 ± 3	0.0167 ± 0.0007

Source: Authors (2021).

It was observed that the degree of sensitization was maintained below 0.5, for all conditions, indicating that no sensitization occurred (Chail & Kangas, 2016). This fact evidences that the passive layer was not disrupted and, therefore, the thermal treatments of aging and solubilization did not alter the resistance to intergranular corrosion of steel. Thus, the presence of phases α', σ and χ did not have significant effect on the degree of sensitization, because of the low precipitation of these deleterious phases, which promoted regions poor in chromium and molybdenum. Additionally, in Figure 6b, two peaks are observed in the activation current, the more noble potential corresponding to the austenite phase, and the less noble corresponding to the ferrite phase.

Figures 7a and 7b show the curves of open circuit potential (OCP) and of cyclic potentiodynamic polarization, respectively, in a 3.5% sodium chloride solution, of steel DSS UNS S31803 under the condition as-received, solubilized, aged at 500°C for 1h and 600°C for 12h.

Figure 7: Corrosion assay of DSS UNS S31803 in a 3.5% sodium chloride solution. (a) Potential in open circuit; (b) Cyclic potentiodynamic polarization.

(a)   (b)
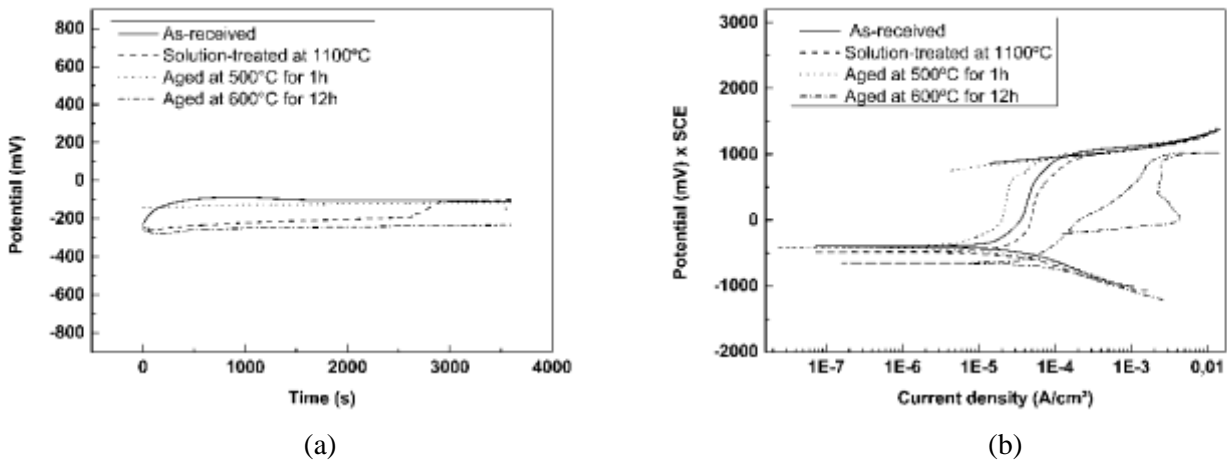
Source: Authors (2021).

From Figure 7a, the values of the corrosion potentials (Ecorr) were obtained, as shown in Table 7. It was observed that under the studied conditions, the values of the potentials increased over time, characterizing the formulation of a passive, stable and adherent layer on the surface of the steel.

Table 7: Open circuit corrosion potential of DSS UNS S31803 in a 3.5% sodium chloride solution.

DSS UNS S31803	Ecorr (mV)
As-received	-114 ± 7
Solution-treated at 1100ºC	-107 ± 4
Aged at 500°C for 1h	-142 ± 6
Aged at 600°C for 12h	-232 ± 4

Source: Authors (2021).

From the polarization curves, Figure 7b, the electrochemical parameters were obtained, by the Tafel's extrapolation method, as shown in Table 8.

Table 8: Electrochemical parameters obtained by cyclic potentiodynamic polarization, of DSS UNS S31803 in 3.5% sodium chloride solution.

DSS UNS S31803	Ecorr (mV)	Epit (mV)	Eprot (mV)	Ipass (A/cm^2)
As-received	-400 ± 8	1056 ± 3	978 ± 9	$(40.9 \pm 1.4) \times 10^{-6}$
Solution-treated at 1100ºC	-440 ± 6	1037 ± 7	1008 ± 3	$(46.9 \pm 2.2) \times 10^{-6}$
Aged at 500ºC for 1 h	-414 ± 1	1038 ± 1	918 ± 2	$(23.5 \pm 0.1) \times 10^{-6}$
Aged at 600°C for 12 h	-604 ± 2	967 ± 8	-148 ± 12	$(11.3 \pm 0.1) \times 10^{-5}$

Source: Authors (2021).

The values of corrosion potential obtained by open circuit were higher than those obtained by the cyclic potentiodynamic polarization curves, Tables 7 and 8, respectively, because the partial removal of the passive layer in the polarization scan started in more negative potentials than the corrosion potential.

The polarization curves show the presence of two passive regions in all conditions tested. This occurred because of the difference in chromium and molybdenum contents between the ferrite and austenite phases, elements that passivate steel. Thus, the ferrite phase that presents higher contents of these elements passivates before the austenite phase.

The values of the electrochemical parameters: corrosion potential (Ecorr), pitting potential (Epit), protection potential (Eprot), corrosion current density (Icorr) and passivation current density (Ipass), under the conditions as-received, solution-treated and aged at 500°C for 1h did not present significant variations, indicating that the precipitation of phase α', present in these conditions, did not affect steel corrosion properties.

Nevertheless, in the treatment of aging at 600°C for 12h, a reduction in the values of corrosion, pitting and protection potential was observed, because of the precipitation of phase sigma (σ) and promoting the formation of regions poor in chromium, and consequently, reducing corrosion resistance. Furthermore, in this condition, higher passivation current density was observed, indicating that the passive layer was formed more slowly than in the other conditions.

Figures 8a and 8b show the micrographs obtained by SEM of DSS UNS S31803, aged at 500ºC for 1h and aged at 600ºC for 12h, respectively, after the assays of corrosion by polarization, in a 3.5% sodium chloride solution. In the two conditions, the localized corrosion by pits was observed, being more intense under the condition aged at 600°C for 12h. The pits were classified as crystallographic (Pit-C), hemispherical (Pit-H) and irregular (Pit-I) and it is noted that pit nucleation occurred preferentially around grain α/α and α/γ and inside the austenite grains, characterizing the selective corrosion.

Figure 8: Micrographs obtained by SEM of DSS UNS S31803, after polarization assays, in a 3.5% sodium chloride solution. (a) Aged at 500ºC for 1h; (b) Aged at 600ºC for 12h.

(a)   (b)
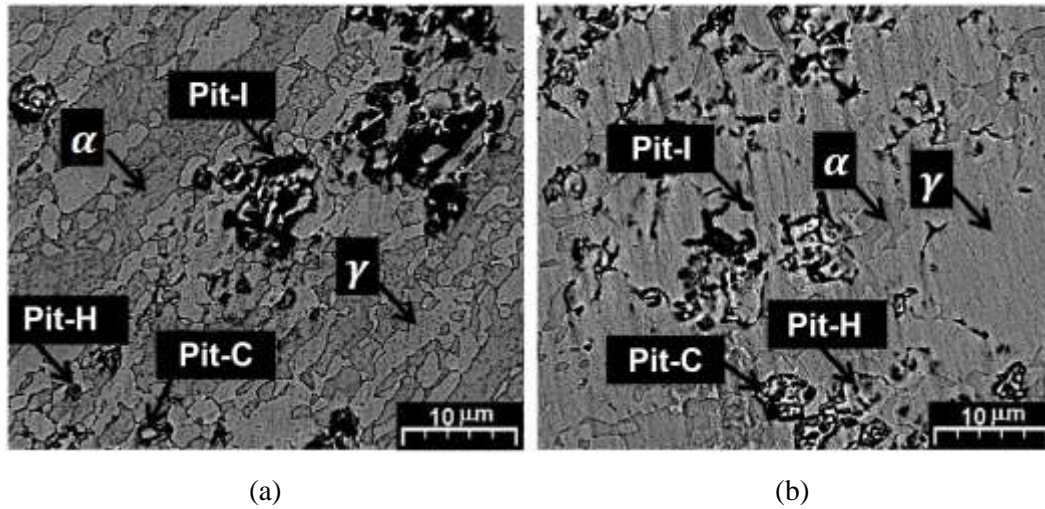
Source: Authors (2021).

Table 9 shows the pitting resistance equivalent number (PREN) of the ferrite and austenite phases, calculated from the chemical composition of the main alloy elements obtained by EDS (Table 2).

Table 9: Pitting resistance equivalent number (PREN) of the phases.

DSS UNS S31803	Phase	PREN
As-received	α	44
	γ	35
Solution-treated at 1100ºC	α	41
	γ	32
Aged at 500°C for 1h	α	49
	γ	37
Aged at 600°C for 12h	α	48
	γ	39

Source: Authors (2021).

It can be observed that a preferential selective corrosion of one of the phases may occur due to the significant difference of the PREN values between the phases. This difference is caused by the non-homogeneous distribution of the passivating elements; consequently, the passive layer can present a different composition between the phases, increasing the probability of occurring defects.

In Figure 8, it is noted that the pits are nucleated around the grains and they grow in ferrite, even with this phase presenting a higher PREN value than austenite. This derives from the fact that the alloy elements Cr and Mo, besides passivators, are stabilizers in the ferrite phase, whereas in the austenite phase they act only as passivators. Therefore, for a corrosion resistance by pits similar to the austenite phase, the ferrite phase should contain higher contents of the elements Cr and Mo.

4. Conclusion

The steel in the condition as-received presented a ferritic matrix with elongated austenite islands and the presence of phases σ and χ. The thermal treatment of solution promoted higher homogenization of the phases and growth of the austenite grains, besides promoting the dissolution of the intermetallic phases σ and χ.

The thermal treatment of aging performed at 500°C for 1h promoted the precipitation of phase α' dispersed in the ferritic matrix, whereas the aging performed at 600°C for 12h, besides the precipitation of phase α', promoted the precipitation of phases σ and χ.

Additionally, the thermal treatments of aging reduced the volumetric fraction of the ferrite phase and/or promoted the precipitation of phases α' and σ, increasing steel hardness.

The ferrite phase of the steels thermally treated by aging at 500°C for 1h and 600°C for 12h presented higher values of microhardness because of α' precipitation. The austenite phase did not undergo significant variation in microhardness, indicating that phase G did not precipitate inside it.

By thermal analysis, the ferromagnetic-paramagnetic transformation of ferrite was observed at 428.9 and 520.4°C, besides ferrite consumption by paramagnetic phases at 842.2 and 860.6°C.

In the tests of double cycle potentiodynamic reactivation, it was observed that the steel did not suffer sensitization under the studied conditions. The open circuit potential assays revealed the formation of a passive and stable film, adherent to the steel surface. By the tests of cyclic potentiodynamic polarization, it was observed that the precipitation of phase α' did not affect corrosion resistance; nevertheless, phase σ reduced corrosion resistance.

In the steels aged at 500°C for 1h and 600°C for 12h, the pits were nucleated around the grains and in the ferrite phase. The ferrite phase presented higher PREN values in relation to austenite, for presenting higher contents of Cr and Mo, which are passivating and alphagenic elements.

In addition, it is important to mention that future studies can be developed in terms of investigation of stress corrosion crack on the conditions evaluated, this topic is little explored in duplex stainless steels. It is also suggested an investigation of reactions resulting from corrosion by electrochemical impedance tests.

References

Alvarez-Armas, I., & Degallaix-Moreuil, S. (2009). *Duplex Stainless Steels*. Wiley.

Appleton, A. (2019). Microstructure Analysis for the Detection of Intermetallic Phases Predictive of Toughness and Corrosion Resistance in Duplex and Lean Duplex Steels. *100 Years of E04 Development of Metallographic Standards*, 166-182.

Arturo, G. R. M., Hugo, L. M. V., Rafael, G. H., Egberto, B. B. & Antonio, G. S. J. (2015). Electrochemical Characterization of AISI 2205 Duplex Stainless Steel Welded Joints with Electromagnetic Interaction. *Procedia Materials Science*, 8, 950-958.

Berecz, T., Fazakas, É., Mészáros, I. & Sajó, I. (2015). Decomposition kinetics of ferrite in isothermally aged SAF 2507-type duplex stainless steel. *Journal of Materials Engineering and Performance*, 24(12), 4777-4788.

Cavalcanti, D. A., Muterlle, P. V. & Reinke, G. (2019). Effect of Sigma Phase Precipitated at 850 °C on Corrosion Behaviour of UNS S82441 Duplex Stainless Steel. *Matéria (Rio de Janeiro)*, 24(3), 1-11.

Chail, G. & Kangas, P. (2016). Super and hyper duplex stainless steels: structures, properties and applications. *Procedia Structural Integrity*, 2, 1755-1762.

Cronemberger, M. E. R. *et al*. (2014). Study of cooling rate influence on SAF 2205 duplex stainless steel solution annealed. *Materials Science Forum*, 802, 398-403.

Cronemberger, M. E. R., Nakamatsu, S., Rovere, C. A. D., Kuri, S. E. & Mariano, N. A. (2015). Effect of cooling rate on the corrosion behavior of As-Cast SAF 2205 duplex stainless steel after solution annealing treatment. *Materials Research*, 18(2), 138-142.

Dille, J. *et al*. (2017). Microstructural evolution during aging at 800 °C and its effect on the magnetic behavior of UNS S32304 lean duplex stainless steel. *Journal of Magnetism and Magnetic Materials*, 426, 102-107.

Haupt, W., Silva, L. E., Falcade, T., Santos, A. C. & Reguly, A. (2019). Effect of ageing time on the toughness and the corrosion properties of duplex stainless steel UNS S31803. *Materials Research*, 22(6), 1-14.

Hilders, O. A., Zambrano, N. & Ochoa, J. L. M. (2018). Microstructural evolution and mechanical property-fractal behavior relations of aged super duplex stainless steel. *Original Research Article*, 27(2), 83-107.

Jinlong, L., Tongxiang, L., Chen, W. & Limin, D. (2015). Comparison of corrosion properties of passive films formed on coarse grained and ultrafine-grained AISI 2205 duplex stainless steels. *Journal of Electro analytical Chemistry*, 757, 263-269.

Kisasoz, A., Gurel, S. & Karaaslan, A. (2016). Effect of Annealing Time and Cooling Rate on Precipitation Processes in a Duplex Corrosion-Resistant Steel. *Metal Science and Heat Treatment*, 57(9-10), 544-547.

Koche, J. C. (2011). *Fundamentos de metodologia científica: Teoria da ciência e iniciação a pesquisa*. Vozes.

Lacerda, J. C., Cândido, L. C. & Godefroid, L. B. (2015). Effect of volume fraction of phases and precipitates on the mechanical behavior of UNS S31803 duplex stainless steel. *International Journal of Fatigue*, 74, 81-87.

Li, X., Lo, K. H., Kwok, C. T., Sun, Y. F. & Lai, K.K. (2018). Post-fire mechanical and corrosion properties of duplex stainless steel: Comparison with ordinary reinforcing-bar steel. *Construction and Building Materials*, 174, 150-158.

Llorca-Isern, N., López-Jiménez, I., López-Luque, H., Biezma, M. V. & Roca, A. (2016). Study of the Precipitation of Secondary Phases in Duplex and Superduplex Stainless Steel. *Materials Science Forum*, 879, 2537-2542.

Ludke, M. & Andre, M. E. D. A. (2013). *Pesquisas em educação: uma abordagem qualitativa*. E.P.U.

Majid, M. & Shahi, A. S. (2020). Influence of intermetallic precipitation on metallurgical, mechanical and pitting behavior of AISI 2205 duplex stainless steel welded joints. *Materials Research Express*, 6(12), 1-23.

Mandal, A. (2016). *Processing-microstructure-microtexture-property correlation of Duplex Stainless Steels* (Thesis). Indian Institute of Technology, Kharagpur, Indian.

Marques, I. J., Silva, F. J. & Santos, T. F. A. (2020). Rapid precipitation of intermetallic phases during isothermal treatment of duplex stainless-steel joints produced by friction stir welding. *Journal of Alloys and Compounds*, 820, 153170.

Martins M. C. & Hara L.C. (2004). Caracterização microestrutural e comportamento à corrosão do aço inox super duplex ASTM A890 GR 6A. In: *59° Congresso Anual da ABM*.

Matias, J. V. S., Tavares, S. S. M., Pardal, J. M. & Ribeiro, R. S. A. (2017). Embrittlement and Corrosion Decay of a Cast Duplex Stainless Steel. *Materials Research*, 20(2), 279-283.

Mehta, M., Jadhav, P., Shaikh, A., Kumar, S. & Kirwai, S. (2019). Effect of Solution Treatment on Microstructure and Mechanical Properties of 2205 Duplex Stainless Steel. *International Journal of Materials, Mechanics and Manufacturing*, 7(6), 254-258.

Mohammed, A. M., Shrikrishna, K. A. & Sathiya, P. (2016). Effects of post weld heat treatment on friction welded duplex stainless steel joints. *Journal of Manufacturing Processes*, 21, 196-200.

Morais, L. C & Magnabosco, R. (2017). Experimental investigations and DICTRA® simulation of sigma phase formation in a duplex stainless steel. *Calphad*, 58, 214-218.

Nithin R. P., Sekar, K. & Joseph, M. A. (2019). Effect of temperature on microstructure evolution and localized corrosion resistance of high tungsten hyper duplex stainless steel. *Materials Research Express*, 6(11), 116557.

Ogawa, K. & Osuki, T. (2020). Modelling of Sigma Phase Precipitation in Super Duplex Stainless Steel Weld Metal. *Isij International*, 60(5), 1016-1021.

Örnek, C., Burke, M., Hashimoto, T., Lim, J. & Engelberg, D. (2017). 475°C Embrittlement of Duplex Stainless Steel - A Comprehensive Microstructure Characterization Study. *Materials Performance and Characterization*, 6(3), 409-436.

Örnek, C. & Engelberg, D. l. (2015). SKPFM measured Volta potential correlated with strain localization in microstructure to understand corrosion susceptibility of cold-rolled grade 2205 duplex stainless steel. *Corrosion Science*, 99, 164-171.

Paulraj, P. & Garg, R. (2015). Effect of intermetallic phases on corrosion behavior and mechanical properties of duplex stainless steel and super-duplex stainless steel. *Advances in Science and Technology Research Journal*, 9, 87-105.

Pereira, A. S., Shitsuka, D. M., Parreira, F. J. & Shitsuka, R. (2018). *Metodologia da pesquisa científica* UFSM.

Powar, A., Gujar, A., Manthani, N., Pawar, V. & Singh, R. (2017). Effect of Secondary Phase Precipitation on Impact Toughness of Duplex Stainless Steel. *Materials Science Forum*, 889, 138-142.

Rezende, S. C., Dainezi, I., Apolinario, R. C., Sousa, L. L. & Mariano, N. A. (2019). Influence of molybdenum on microstructure and pitting corrosion behavior of solution-treated duplex stainless steel in a lithium chloride solution. *Materials Research*, 22(1), 1-11.

Rezende, S.C. *et al*. (2018). Effect of solution annealing time on the microstructure and corrosion resistance of duplex stainless steel. *Materials Science Forum*, 930, 374-379.

Rivolta, B., Gerosa, R. & Tavasci, F. (2018). The dilatometric technique for studying sigma phase precipitation kinetics in F55 steel grade. *Journal of Thermal Analysis and Calorimetry*, 132(2), 869-877.

Sáenz, L. *et al*. (2020). Duplex Stainless Steel Subjected to Normalized Thermal Treatment. *Key Engineering Materials*, 834, 103-109.

Santos, D. C. & Magnabosco, R. (2015). Kinetic Study to Predict Sigma Phase Formation in Duplex Stainless Steels. *Metallurgical and Materials Transactions A*, 47(4), 1554-1565.

Sicupira, D. C., Cardoso Junior, R., Bracarense, A. Q., Frankel, G. S. & Lins, V. F. C. (2016). Electrochemical study of passive films formed on welded lean duplex stainless steel. *Materials and Corrosion*, 68(6), 604-612.

Silva, E. *et al*. (2016). Classification of Induced Magnetic Field Signals for the Microstructural Characterization of Sigma Phase in Duplex Stainless Steels. *Metals*, 6(7), 164-180.

Silva, R. *et al*. (2016). Effect of thermal aging at 475 °C on the properties of lean duplex stainless steel 2101. *Materials Characterization*, 114, 211-217.

Valeriano, L. C., Correa, E. O., Mariano, N. A., Robin, A. L. M. & Machado, M. A. G. T. C. (2019). Influence of the Solution-Treatment Temperature and Short Aging Times on The Electrochemical Corrosion Behaviour of Uns S32520 Super Duplex Stainless Steel. *Materials Research*, 22(4), 1-7.

Verma, J. & Taiwade, R. V. (2017). Effect of welding processes and conditions on the microstructure, mechanical properties and corrosion resistance of duplex stainless steel weldments A review. *Journal of Manufacturing Processes*, 25, 134-152.

Warren, A. D. *et al*. (2015). Quantification of sigma-phase evolution in thermally aged 2205 duplex stainless steel. *Journal of Materials Science*, 51(2), 694-707.

Xiang, H., Liu, C., Deng, L. & Zheng, K. (2019). Effect of Aging Temperature on the Microstructure and Properties of Economical Duplex Stainless Steel. *Materials*, 12(13), 2085.

Zeng, H., Yang, Y., Xu, R., Xin, S. & Li, M. (2019). Pitting corrosion resistance of sensitized type 2205 duplex stainless steel in hot concentrated seawater. *Journal of Solid State Electrochemistry*, 23, 2793-2801.

Zhang, Z. *et al*. (2017). Influence of microstructure and elemental partitioning on pitting corrosion resistance of duplex stainless steel welding joints. *Applied Surface Science*, 394, 297-314.